Challenging Glass Conference Proceedings – Volume 10 – June 2026 – Louter, Bos & Belis (Eds.)
International Conference on the Architectural and Structural Application of Glass
Challenging Glass Conference 10 – 15-17 June 2026 – TU Delft – The Netherlands

Evaluating Trade-Offs Between Embodied Carbon Production and Projected Reductions in Operational Carbon Achieved by Façade Retrofit

Daniel Bettenhausen, James Casper, Adam Krueger

Enclos, United States, dbettenhausen@enlcos.com, jcasper@enclos.com, akrueger@enclos.com

Abstract

Strategies for reducing carbon emissions associated with commercial buildings are realized by either tracking emissions that correspond to the production, installation and replacement of building materials or tracking emissions that correspond to the occupied use of the building through utility monitoring. These approaches are distinguished respectively as considering “embodied” and “operational” carbon. The focus of this paper is to evaluate the net balance that is achieved when the embodied carbon associated with a specific façade installation is compared with the potential savings in carbon emissions that result from its deployment. This study follows the net energy transfer associated with a given unitized façade unit in different climates in accordance with existing weather records and for various building orientations. Recognition is given to potential improvements in thermal performance achieved by reducing air leakage, improving assembly U-factor and enhancing solar control. The results are evaluated in the context of existing environmental product declarations for the replacement façade and fuel sources corresponding to space conditioning with the goal of determining under what circumstances façade retrofit provides a viable path to reducing emissions.

Keywords

Sustainability, Embodied Carbon, Operational Carbon, Façade Retrofit, Thermal Design

Article Information

- Digital Object Identifier (DOI): 10.47982/cgc.10.677
- Published by Challenging Glass, on behalf of the author(s), at Stichting OpenAccess.
- Published as part of the peer-reviewed Challenging Glass Conference Proceedings, Volume 10, June 2026, 10.47982/cgc.10
- Editors: Christian Louter, Freek Bos & Jan Belis
- This work is licensed under a Creative Commons Attribution 4.0 International (CC BY 4.0) license.
- Copyright © 2026 with the author(s)

Nomenclature

Variable	Description	Units
q'	Heat transfer rate per unit of projected wall area	W/m^2 (Btu/hr-ft^2)
U	U-Factor (Conductance)	W/m^2-C (Btu/hr-ft^2-F)
A	Area	m^2 (ft^2)
V	Wind velocity	m/s (ft/s)
T	Temperature	C (F)
ΔT	Interior-exterior temperature difference	C (F)
k	Thermal conductivity	W/m^2-C (Btu/hr-ft^2-F)
x, y	Spatial coordinates	m (ft)
h	Surface coefficient of convective heat transfer	W/m^2 (Btu/hr-ft^2)
I	Incident solar radiation	W/m^2 (Btu/hr-ft^2)
A_i	Anisotropy index	
R_b	Ratio of beam radiation on a tilted surface to a horizontal surface	
δ	Solar declination	
$\emptyset$	Latitude	
β	Panel inclination	
ω	Hour angle	
n	Day of year	
θ	Angle of incidence relative to panel surface	
θ_z	Angle of separation between beam radiation and zenith	
t	Time of day	Hour of Day
p	Pressure	Pascals (PSF)
ρ	Mass density	kg/m^3 [lbm/ft^3]
c_p	Specific heat capacity at standard pressure	J/kg-C [btu/lbm-F]
$SHGC$	Solar heat gain coefficient	
WWR	Window to wall ratio	
EER	Energy efficiency ratio	Btu/hr-watt
ρ_g	Surface Albedo	

Subscripts

f_n	Component of framing n
e_n	Component of glass edge n
c_n	Component of glazing center n
w	For exterior wind
T	For tilted surface
b	Beam component
d	Diffuse component
Sol	Solar

Lc	Local correction
Eot	Equation of time
Inf	Corresponding to air infiltration
θ	At angle of incidence
$\bar{\theta}$	According to the hemispherical average

1. Introduction

In recent decades, the relationship between human activity and changes in climate patterns have been studied, analyzed and discussed resulting in a voluminous work of literature. (M. Lynas, et. al. 2021). Those efforts, and many emerging studies, are motivated by the growing consensus that atmospheric temperatures are currently rising in a manner that poses risks to the health and well-being of both present and future generations (H. Pörtner, et. al. 2022). Acting in chorus, strategies have been proposed by design professionals to address a growing market for new products, construction practices and building retrofit work that diminishes the production of greenhouse gas (GHG) emissions. In particular CO_2 gas, a common byproduct of manufacturing and building operation, is widely targeted, since it incumbers the long-wave dissipation of thermal radiation away from the earth's surface. This emission constitutes a critical mechanism required to maintain stable atmospheric temperatures that would otherwise rise due to imbalanced solar incidence. Efforts to mitigate CO_2 emissions focus on either the production, installation and demolition of materials, commonly categorized as embodied carbon or by reducing the energy consumption of buildings associated with utility loads through material selection and design, which is referred to as operational carbon. Efforts to enforce sustainable building design can consider either source. For instance, in the United States Local Law 97 (City of New York, 2019) aims to reduce carbon reduction through utility use monitoring and associated carbon production whereas the Buy Clean California Act (State of California, 2022) focuses on transparency in embodied carbon by requiring carbon intensive construction materials to undergo a life cycle assessment to reveal their global warming potential. In both cases the long-term aim is to enforce thresholds on carbon emission. These two examples are clearly not an exhaustive list of initiatives aimed at regulating carbon accounting in the construction industry but highlight a key difference in the way the subject can be approached.

Existing buildings must be examined under a different lens than new construction since the GHG emissions associated with their inherent materials have already been released. This naturally leads us to question under what circumstances modifications aimed at increasing the energy efficiency of a building will yield a net reduction in GHG emissions over the lifetime of the building when the additional embodied carbon associated with renovation or retrofit work is accounted for? Policies with a sole focus on either embodied or operational carbon may fall short of realizing a net carbon reduction. The aim of this paper is to develop a simplified analytical framework to address this question.

Accounts within the published literature have attempted to characterize the relationship between operational and embodied carbon in buildings. A recent study by (T. Srisamranrungruang and K. Hiyama, 2026) analyzed various specific façade deployments in the climate of Japan and concluded that over a thirty-year time period that, in many instances, operational carbon associated with the façade exceeded embodied carbon associated with the materials observing sections A1-A3 of the product life cycle defined per EN15978. It is unclear whether these findings would apply to other climates where heating loads are more significant? (T.M. Echenagucia and T. Moroseaos, et. al., 2023)

performed building energy simulations with different façade deployments in 6 U.S. cities and concluded that that tradeoffs were localized depending largely on the carbon intensity of electrical utilities. The study observed steel framed walls and specific HVAC equipment in medium sized buildings. Energy expenditure was calculated in the context of the entire building including heat transfer at locations exceeding the façade elements. It is reasonable to question if a comparable analysis could be performed for larger buildings with different fenestration types? (Rosanna O'Neill, et. al., 2021) presented as study of a building in Queensland Australia considering embodied energy, operational carbon and cost. As with the case of (T. Srisamranrungruang and K. Hiyama, 2026) the results correspond to a specific mild sub-tropical environment. The study determined that low-emissivity coatings provided the greatest economy for achieving carbon reduction versus other material enhancements. (Robert Giordano et. al. 2017) considered various façade configurations and the impact of a given material selection on total building operational carbon. Their study also concluded that tradeoffs in embodied and operational energy were sensitive to climate. In these instances, the outcomes were tied to specific buildings with results derived from energy modeling and the energy balances were not directly correlated with GHG emissions.

2. Mathematical Model

The aim of the study presented herein is to propose a mathematical framework for assessing the time frame over which reductions in building energy use that are directly attributable to the façade, whether those are realized through renovation or replacement, are sufficient to offset the embodied carbon associated with their deployment. The time period will henceforth be defined as the "carbon payback period." This analysis is particularly relevant if large portions of the exterior façade are replaced since aluminum and glass exhibit significant quantities of embodied carbon. This approach requires first that the net value of energy transfer associated with a given façade element is quantified over a significant enough period of time to consider variations in weather and solar conditions. These loads can then be categorized as contributing to either heating or cooling and weighed against the embodied carbon associated with their respective utility energy sources and mechanical system efficiencies. It is not the aim of the study to provide a totally comprehensive evaluation of every factor which might influence this balance. For instance, the geometry of a given building, the use of shading devices, variations in interior volume, specific HVAC designs and various other factors need to be evaluated in a specific case. The framework presented here instead aims to empower development of comparative tools that can be employed early in project design phases to analyze tradeoffs specific to given wall system designs using analysis tools that are already commonly required to be used per model energy codes in the United States. Specifically, it is the convention of the industry in the United States to observe engineering standards curated by the National Fenestration Ratings Council (NFRC) to determine the thermal transmittance of building envelope elements since those standards are citied in the most widely adopted model energy code (ASHRAE 90.1, 2022). Within the context of this standard the net energy balance acting on a façade element is underpinned by ratings for U-factor, Solar Heat Gain Coefficient (SHGC) and air infiltration. While the mechanisms of fluid mechanics and heat transfer which underly these ratings are intertwined, they are evaluated separately under discrete sets of environmental conditions for the sake of efficiency. This is regarded as a necessary simplification to facilitate engineering calculations.

2.1. U-Factor

The U-Factor of the building envelope is the constant of proportionality that represents the conductance of the envelope to heat transfer that results from the temperature difference imposed at its interior and exterior boundaries. This relationship is defined in (Eq. 1). Within the scope of the standard, the area encompassing a window, door or any other planar fenestration component is further subdivided into discrete elements representing the frame *f,* the glass-center *c,* and the glass-edge *e* where the frame and glass interact as described in (Fig. 1) and (Eq. 2). It is noteworthy that this nomenclature was established at a time when the standard only considered vision glass. It has since been expanded to include opaque wall areas such as doors, opacified spandrel and other wall elements.

The area corresponding to each element is that which is projected normal to the plane of glass and demised by the sightline of the frame at its interface with the glazing. For windows, the glass edge is defined as the first 63.5 mm (2.5”) of distance extending inwards from the site line towards the center of the glass. For opaque wall, 254 mm (10”) of edge distance is included if the assembly is in-filled with insulation since such assemblies sometimes include a conductive metal back pans for fire protection and resilience to damage in the field.

The U-factors corresponding to each element account for the summation of the rate of heat transfer over the complete extent of the internal boundary. Since the calculations are steady state, this approach is mathematically conservative in relation to the total rate of heat transfer that would otherwise be calculated over the exterior boundary.

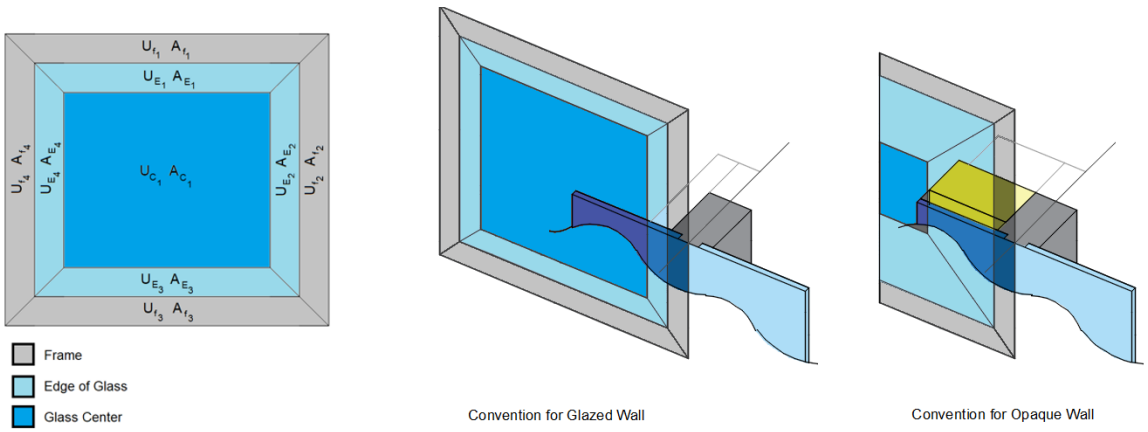

Fig. 1: Elements Considered in U-factor Calculations.

$$q' = U\Delta T \qquad \text{(Eq. 1)}$$

$$U = \frac{1}{A}\left[\sum_{i=1}^{n} U_{f_n} A_{f_n} + \sum_{i=1}^{n} U_{e_n} A_{e_n} + \sum_{i=1}^{n} U_{c_n} A_{c_n}\right] \qquad \text{(Eq. 2)}$$

Heat transfer calculations vary in accordance with the zones identified. Throughout the framing and edge regions the nature of the heat transfer is approximated to be 2-dimensional corresponding to cross-sections of the frame; whereas, at the glass center a 1-dimensional calculation is employed. These assumptions are justified, within the context of the accuracy required of an engineering standard, by the fact that most frame components are extruded continuously over the length of a given

mullion or transom with only a select number of intermittent parts and heat transfer through the glazing is largely unaffected by the frame beyond the glass edge region. Even though the junction of framing materials at corners, and other conditions might invoke heat transfer to occur out of plane, this simplification has not been shown to result in errors exceeding 10% in relation to testing per (ASTM C1199, 2022) for test configurations dictated by (NFRC/ANSI-100, 2023) A more detailed investigation of these sensitivities would be a rational extension of this work.

The NFRC 100 standard specifies that these calculations be conducted with specific software programs that conform to (ISO15099, 2022). These programs are named THERM and WINDOW. They were produced and are maintained by the Window and Daylighting group of Lawrence Berkley National Laboratory (LBNL) in the United States. THERM is employed for 2-dimensional modeling of frame components and WINDOW produces 1-dimensional analysis of the glazing. Since a detailed account of the mathematical formulation and calculation procedures is provided by (ISO15099, 2022) and (LBNL, 2026) it would be redundant to provide more than a basic description here. The THERM program employs Finite Element Analysis (FEA) observing the governing equation of heat conduction in the steady state (Eq. 3). All modes of heat transfer within the solution domain boundaries are represented as conduction. The influence of convection and radiation within this zone is approximated by utility of an effective conductivity. Radiation at the interior boundary employs view factor calculations and radiation at the exterior boundary assumes the view factor is unity with isothermal surroundings in both cases. The remaining boundary conditions employ a heat transfer coefficient to represent convection. This latter reality deserves emphasis because the NFRC standard enforces specific environmental conditions. In particular, a 5.5 m/s exterior wind velocity is assumed, and natural convection is assumed at internal surfaces. These coefficients are intimately connected to the U-factors reported. Low exterior wind speeds and actual perimeter space conditioning can result in significant variations. Since wind speeds are well represented in weather records, the U-factor of a given façade element calculated in accordance with NFRC calculation procedures is modified in accordance with (Eqs. 4 and 5) where V is the wind velocity in m/s and U_w is the wind adjusted U-factor in W/m^2-K.

$$k\left(\frac{\partial^2 T}{\partial x^2}+\frac{\partial^2 T}{\partial y^2}\right)=0 \qquad \text{(Eq 3.)}$$

$$h_w(V)=4V\ +4 \qquad \text{(Eq 4.)}$$

$$U_w=\left[U^{-1}\ +{h_w}^{-1}-0.04\right]^{-1} \qquad \text{(Eq 5.)}$$

2.2. Solar Gain

The solar heat gain coefficient at a given angle of incidence Θ ($SHGC_\Theta$), is defined according to (ANSI/NFRC 300, 2023) as the portion of incident solar heat flux that is transferred through a fenestration element corresponding to that angle of incidence. Unlike THERM, which employs a field equation to solve for the temperature distribution throughout the solution domain, WINDOW solves for the temperature at nodes bounding each glazing layer in a manner that considers absorption within the layer, conduction through the material and the radiosity at its surfaces. Convection within glazing cavities follows similar conventions to those employed in THERM whereby an affective conductance is

calculated. The spectral properties of the glass for various incidence angles are obtained from measurement of the resulting transmission spectrum when the glazing is exposed to an (ISO9845, 2022) solar spectrum, also known as the air mass 1.5 spectrum.

To facilitate accurate heat transfer calculations the magnitude of the incident solar radiation and its angle of incidence must be determined. Solar conditions vary geographically, with time and are also sensitive to atmospheric conditions. A common approach employed to predict solar insolation on a tilted surface I_T relies upon recorded measurements of incident solar radiation on a horizontal terrestrial plane and a geometric model to account for the difference in orientation. The forthcoming results of this study observe one such model, the (Hay and Davies, 1980) solar radiation model (Eq 6.)

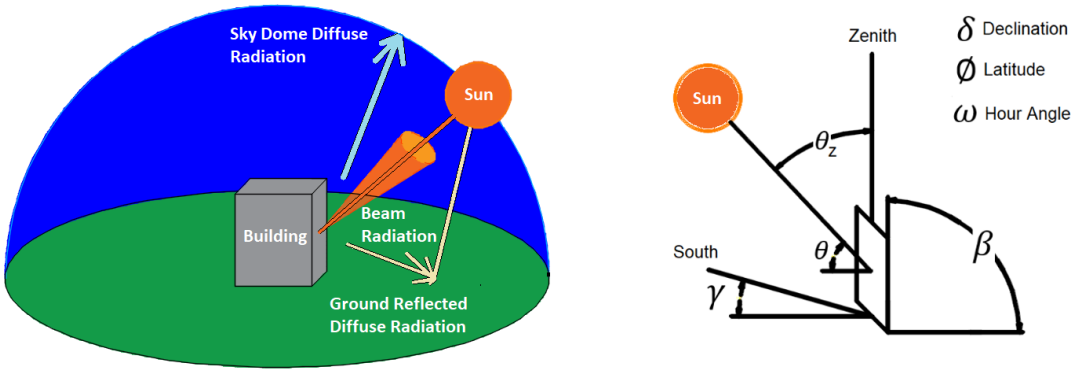

Fig. 2: Solar Geometry.

The model defines an anisotropic sky accounting for the effects of circumsolar radiation and ground reflected radiation as depicted in (Fig. 2). The solar data required as inputs to the model were acquired from the National Solar Radiation Database (NREL, 2026) for the year 2024 which is the most recent record.

$$I_T = (I_b + I_d A_i) R_b + I_d (1 - A_i) \left(\frac{1+cos\beta}{2}\right) + I\rho_g \left(\frac{1-cos\beta}{2}\right) \quad \text{(Eq. 6)}$$

$$A_i = \frac{I_b}{I} \quad \text{(Eq. 7)}$$

$$R_b = \frac{I_{bT}}{I_b} = \frac{\cos(\theta)}{\cos(\theta_z)} \quad \text{(Eq. 8)}$$

$$\cos(\theta) = \sin(\delta)\sin(\emptyset)\cos(\beta) - \sin(\delta)\cos(\emptyset)\sin(\beta)\cos(\gamma) \quad \text{(Eq. 9)}$$

$$+ \cos(\delta)\cos(\emptyset)\cos(\beta)\cos(\omega) + \cos(\delta)\sin(\emptyset)\sin(\beta)\cos(\gamma)\cos(\omega)$$

$$+\cos(\delta)\sin(\beta)\sin(\gamma)\sin(\omega)$$

$$\delta = 23.45\, sin\left(360\frac{284+n}{365}\right) \quad \text{(Eq. 10)}$$

$$t_{sol} = t_{lst} + t_{lc} + t_{eot} \quad \text{(Eq. 11)}$$

$$t_{lc} = 4 * (\emptyset - \emptyset_{std\ mer})\ [min] \quad \text{(Eq. 12)}$$

$$t_{eot} = 229.2\begin{pmatrix}0.000075 + 0.001868\cos(B) - 0.032077\sin(B)\\ -0.014615\cos(2B) - 0.04089\sin(B)\end{pmatrix}, \quad \text{(Eq. 13)}$$

$$B = (n-1)\frac{360}{365}$$

The terms I_b and I_d correspond to the beam and diffuse components of solar insolation over the period of an hour on a horizontal plane. It is noteworthy that measurements of beam insolation contained within NSRDB hourly datasets correspond to a plane perpendicular to the angle of incidence, so the equation cannot be applied directly. The anisotropy index A_i (Eq. 7) represents the fraction of the total horizontal insolation that corresponds to the beam component. Under clear sky conditions the value of A_i is near unity which assigns most of the diffuse component to be regarded as beam radiation; whereas, when skies are cloudy the radiation is modeled as being almost entirely diffuse since I_b is also very low under that condition. Spanning these conditions, some portion of the diffuse radiation is regarded as being, "forward scattered" and attributed to the beam component. It is noteworthy that the distinction between insolation of beam and diffuse origin, the first two terms in the equation, is significant because different geometric treatments are required when extrapolating values from a horizontal surface to one that is inclined with a specific cardinal orientation. For beam radiation, the location of the sun in the sky must be considered relative to the surface of interest, whereas treatment of the diffuse component need only consider the fraction of solar radiation that is shaded by the horizon. The 3rd term containing the coefficient ρ_g, the ground surface albedo, represents ground reflected radiation below the horizon. For the purposes of this study ρ_g was assumed to be 0.25 which would be characteristic of most urban settings.

The treatment of beam radiation evokes the coefficient R_b which is the ratio of solar radiation incident at any surface I_{bT}; that which is sloped at an angle above the ground plane β, and for any surface azimuth angle ϒ, to the portion of the beam component that is received horizontally at the referenced measurement surface I_b. The convention observed for ϒ is that south and north are respectively defined as 0° and 180° with negative values corresponding to east facing orientations and positive values corresponding to western orientations. Since the present study considers vertical façade elements β is 90° and the surface of interest will be henceforth referred to as the façade. R_b is given by (Eq. 8). The terms cos(Θ) and cos(Θ_z), where Θ spans the angle between the direction of beam radiation and the surface normal of the vertical façade. Θ_z is the angle which separates the direction of the suns position in the sky to the ground plane. These trigonometric relationships are derived from (Eq. 9).

For the application in question, β, the inclination of the façade, ϒ, the cardinal orientation of the facade and the previously undefined latitude at the location of the building ϕ can be regarded as constants for a given installation. The solar declination δ and hour angle ω vary with time throughout the year and by day. The declination angle accounts for the variation of the sun's path through the sky during different seasons since the earth's axis of rotation is tilted as it orbits the sun. For these solar calculations (Eq. 10) provides a sufficiently accurate approximation of δ where n is the day of the year. The hour angle ω indicates the position of the sun east or west of the local meridian throughout a given day moving at a rate of 15 degrees per hour and with 0 degrees corresponding to local solar time at noon, the point in time at which the sun is "overhead" coinciding with the local meridian of the observer. Local solar time, (Eq. 11) is adjusted from local standard time with additional terms to account for corrections in longitude (Eq. 12) and the elliptical path of the sun's orbit, the latter adjustment is also commonly described as the "equation of time." (Eq. 13)

2.3. Air Infiltration

Ventilation and air infiltration have a significant impact on HVAC loads. In most cases ventilation is desirable to offset solar gain unless it is purposefully deployed to correct deficiencies in space conditioning management. For example, tenants opening windows during heating conditions to correct for overruns in HVAC setpoints. Air infiltration is uncontrolled ventilation due to air leakage through gaps in gaskets, poor or missing sealant work, errors in fitment and other deficiencies that are either inherent to new installations or, as is more often the case, occur due to aging and wear on system components. In heating climates air leakage can contribute significantly to moisture management issues such as condensation and water leakage. It furthermore taxes HVAC systems.

When properly installed, most window systems exhibit low air leakage rates. A common test specification employed for curtain wall is 0.03 LPS/m^2 (0.06 CFM/ft^2) at 47.9 Pa (6.24 PSF). For structurally glazed curtain wall systems tests often simply report that actual values are below this specification since the actual leakage rates are too small to accurately measure. Building commissioning requirements, such as full building blower door testing per (ASTM E779, 2019) all but ensure that modern construction is relatively tight when newly installed. Air leakage rates corresponding to aging installed work are more difficult to access since they are not routinely measured.

Energy use associated with air infiltration depends on the pressure difference between interior and exterior conditions. This relationship is very complex because the interaction of wind and a given building results in a flow field with regions of high and low pressure relative to the building interior which may exhibit its own variations in accordance with HVAC operation, stack effect and the extent that the building is sealed from external pressure influences. It can be stated generally that leakage rates increase with wind action. As a rough approximation the stagnation pressure (Eq. 14) associated with weather data provides an estimate that can be easily calculated from weather records.

Heat transfer associated with the resulting flow rate can be most easily calculated in accordance with test data establishing the function $\dot{m}_{\Delta p}$ for the representative area. Since infiltration counters HVAC operation it is reasonable to consider it as an energy loss relative to fuel and power consumption under all circumstances. The relationship between heat transfer and flow rate is shown in (Eq. 15).

$$\Delta p = \frac{1}{2}\rho v^2 \qquad \text{(Eq. 14)}$$

$$Q_{inf} = \dot{m}_{\Delta p} c_p (T_e - T_i) \qquad \text{(Eq. 15)}$$

The model presented considers temperature driven heat transfer, solar heat transfer and energy loss due to air infiltration. The net energy balance is given by (Eq. 16) where the window to wall ratio (WWR) is the portion of the system with transparent glazing. Heat gain through spandrel areas, which are completely backed with insulation, were considered to be negligible in relation to solar transfer through the vision glass.

$$Q = |U_w A(T_e - T_i) + I * WWR| + \left|\dot{m}_{\Delta p} c_p (T_e - T_i)\right| \qquad \text{(Eq. 16a)}$$

$$I = SHGC_\theta (I_b + I_d A_i) R_b + SHGC_{\bar{\theta}} \left(I_d (1 - A_i) \left(\frac{1+cos\beta}{2}\right) + I\rho_g \left(\frac{1-cos\beta}{2}\right)\right) \qquad \text{(Eq. 16b)}$$

3. Modelled Scenarios

The study presented herein considers the application of this model to 6 cities with varying climates as depicted in (Table 1).

Table 1: Geographic Scope of Analysis

City	State	ASHRAE Climate Designation
New York	New York	Mixed Humid
Minneapolis	Minnesota	Cold Humid
Denver	Colorado	Cool Dry
Seattle	Washington	Mixed Marine
Las Vegas	Nevada	Warm Dry
Miami	Florida	Very Hot Humid

In each case weather data was obtained from the National Solar Radiation Database (NREL, 2026) for the year 2024. These records include solar conditions, ambient temperature and wind speed at hourly intervals for the entire calendar year. 2024 is the most current complete record.

The representation of a reclad system is depicted in (Fig. 3 and 4)**.** (Fig. 3) depicts the primary curtain wall details and (Fig. 4) shows the system in Elevation. This system was chosen due to the nature of its conventional thermal enhancements and the fact that the GWP of the system has been analyzed and reported, (ICC Evaluation Service, 2021). The system consists of a thermally broken unitized curtain wall with unit dimensions of 1.52 [m] (5 [ft]) in width, 4.57 [m] (15 [ft]) in height and a WWR of approximately 66%. It is the experience of the author that this deployment, allowing for some level of variation is conventional of many buildings in the United States.

The glass make-up observed for the study was the same in both vision and spandrel areas consisting of a 25 mm insulating glass make up with 6 mm glass plies, 2nd surface triple silver coating, 90% argon gas fill and true warm edge, “foam” spacers. The spandrel areas are insulated with 4” of mineral wool insulation and 2” depth field applied insulation, “mullion wraps” applied only over the vertical framing, overlapping the assembly insulation by 2”. The spandrel areas include a 20-gauge galvanized steel back pan with, “returned leg” attachment to the framing.

The U-factors corresponding to the vision area and spandrel area including the supplemental field insulation are respectively 1.93 [W/m^2-K] (0.34 [Btu/hr-ft^2-F]) and 0.62 [W/m^2-K] (0.11 [Btu/hr-ft^2-F]). It is noteworthy, U-Factors reported in NFRC product certifications commonly indicate results corresponding to a standard specified elevation size and mullion deployment that does not reflect the installed dimensions. In this case the actual unit dimensions corresponding to the environmental product declaration were observed in U-factor calculations for the sake of accuracy. The combined U-factor for a typical unitized curtain wall assembly based on these values is 1.47 [W/m^2-K] (0.26 [Btu/hr-ft^2-F]). Other metrics corresponding to this base system required to underpin the analysis include the SHGC of the glazing. Those values, tabulated for different incidence angles, are provided in (Table 2). The relationship between air infiltration rate and wind pressure is assumed to be linear over the range of non-extreme wind pressures that are relevant. Within this regime, leakage through gaskets and other small orifices is likely governed by frictional losses and reasonably approximated as exhibiting a linear relationship with velocity. The relation is established such that the leakage rate is zero in the absence of wind and 0.03 LPS/m^2 (0.06 CFM/ft^2) at a pressure of 47.9 Pa (6.24 PSF). As described in

the foregoing, pressure is established as the stagnation pressure corresponding to wind velocity from the NSRDB records.

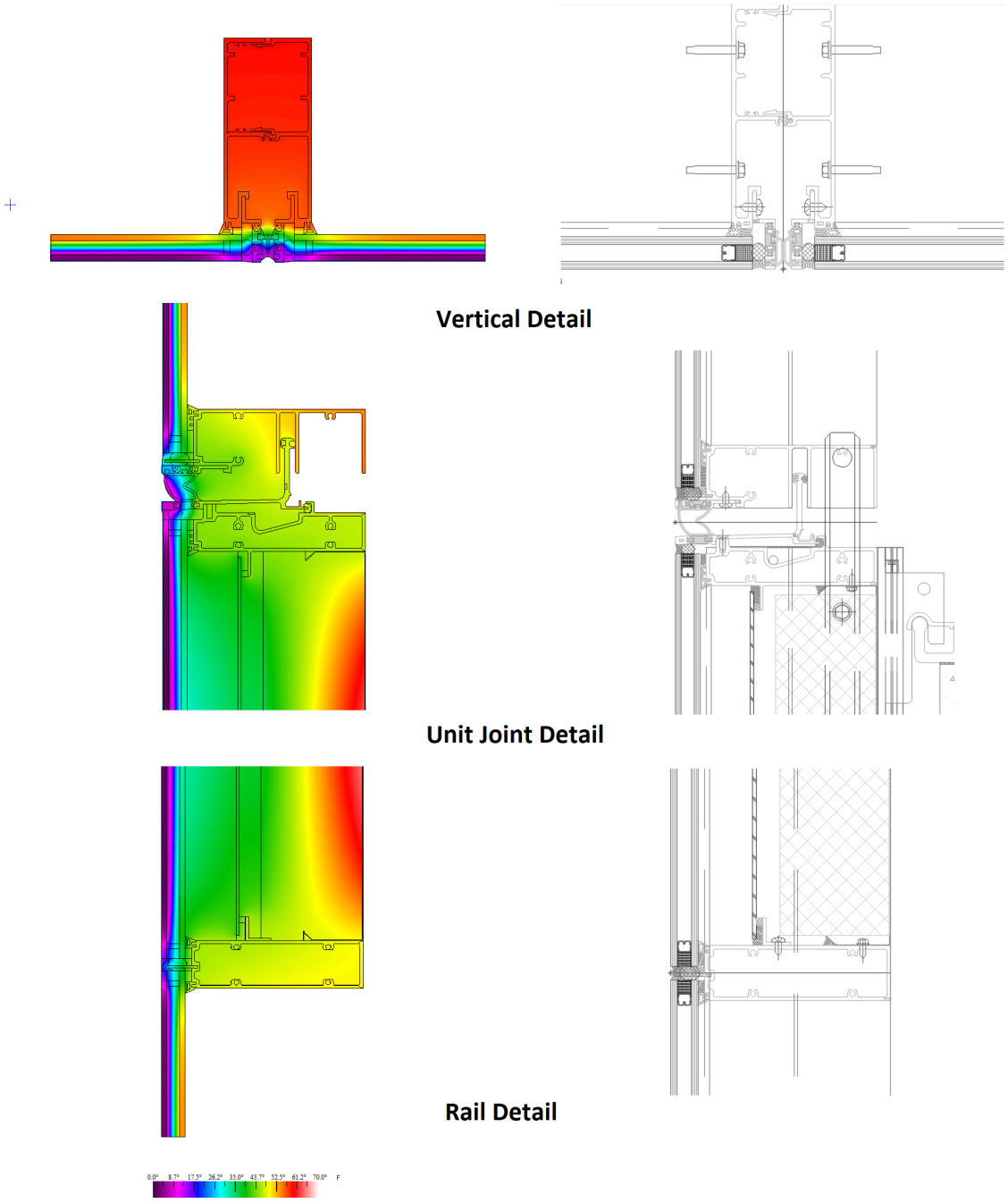

Fig. 3: EPD1044 System Details and Color Contour Diagrams of Temperature.

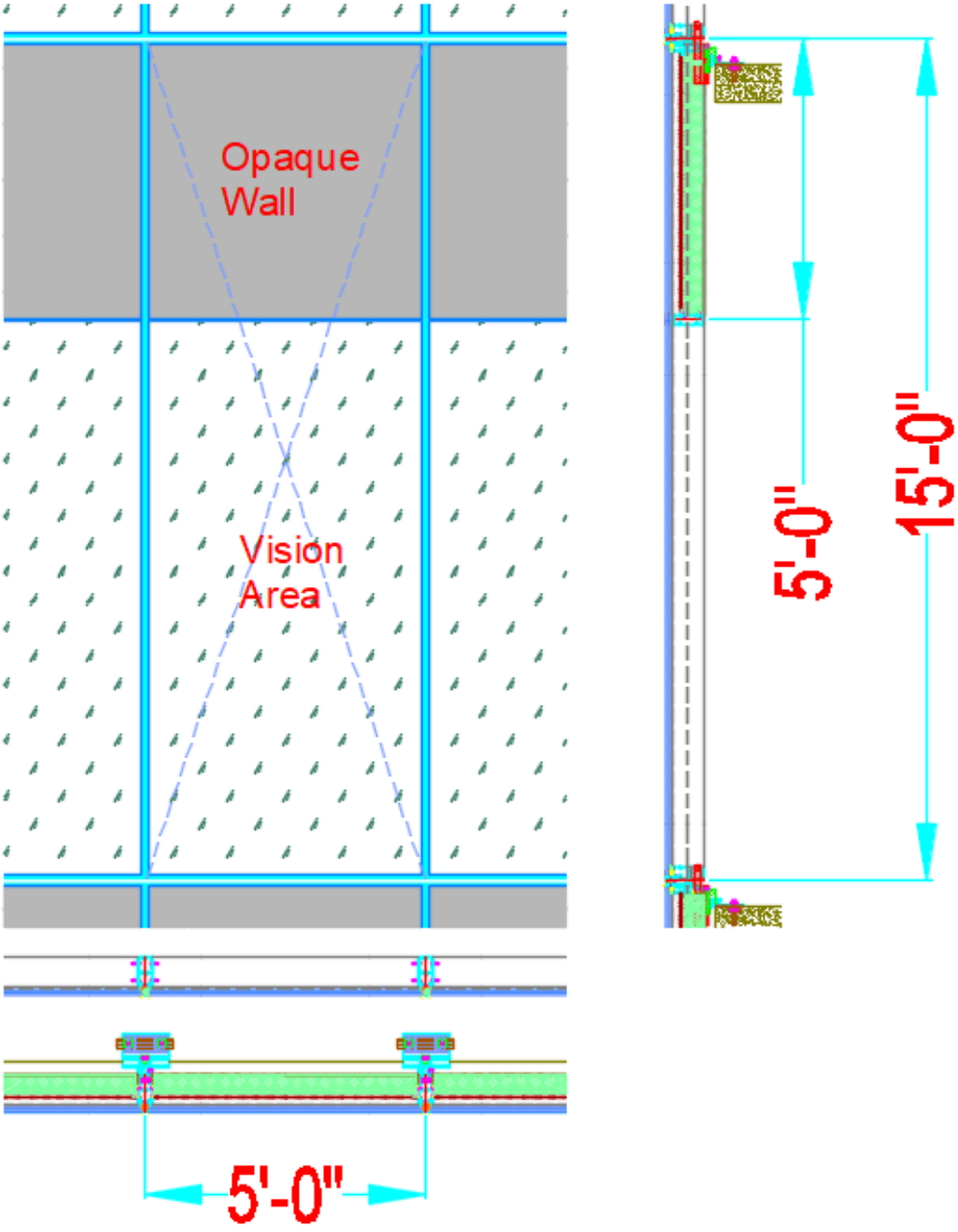

Fig. 4: Curtain Wall Unit Elevation and Dimensions.

Performance metrics corresponding to existing construction are more difficult to establish. Since it is unlikely that newer or high performing systems would be arbitrarily replaced, the nature of most candidates for façade retrofit exhibit features such as poor performing monolithic glass, damaged gasket systems, loose operators and framing systems that do not employ modern thermal improvements. In some cases, these systems may feature renovations that were added to improve their performance and appearance. Examples include polishing glass, applying or replacing solar control films, arresting failed operators with mechanical restraints, replacing sealant work and possibly adding insulation. These provisions are lucrative to owners and tenants if they can be performed

without decommissioning interior space, performing activities outside of the building, or needing to disrupt and replace interior finishes. Subsequently they would rarely entail glass replacement, revisions to framing systems or insulation that is "walled in." It would be shortsighted to ignore such improvements when evaluating the potential for carbon parity. Thus, three systems were included in the evaluation as depicted in (Table 2.)

Table 2: Analysis Cases

	Reclad with ES EPD1044	Renovated	Unimproved Existing
Description	Representitive of New Construction	Sealed to Mitigate Air Infiltration and Solar Control Film Applied to Glazing	Uncoated Monolithic Glazing and No Improvements
Glazing	Insulated Glass with Triple Silver Coating, Argon and Warm Edge Spacers	Monolithic Glass with Applied Solar Control Film	Monolithic Glass
Unit Width	1.52 [m] (5 [ft])	1.52 [m] (5 [ft])	1.52 [m] (5 [ft])
Unit Height	4.57 [m] (15 [ft])	4.57 [m] (15 [ft])	4.57 [m] (15 [ft])
WWR	65%	65%	65%
U-Factor of Vision (Assembly)	1.93 [W/m^2-K] 0.34 [Btu/hr-ft^2-F]	5.11 [W/m^2-K] 0.90 [Btu/hr-ft^2-F]	5.11 [W/m^2-K] 0.90 [Btu/hr-ft^2-F]
U-Factor of Spandrel (Assembly)	0.62 [W/m^2-K] 0.11 [Btu/hr-ft^2-F]	1.14 [W/m^2-K] 0.20[Btu/hr-ft^2-F]	1.14 [W/m^2-K] 0.20 [Btu/hr-ft^2-F]
Air Infiltration [LPS/m^2] at 50 [Pa]	0.03	0.03	0.12
Solar Coating	Triple Silver	Silver Reflective Film	None
SHGC(Θ)			
0	0.223	0.216	0.818
10	0.225	0.217	0.817
20	0.223	0.217	0.815
30	0.219	0.215	0.81
40	0.215	0.212	0.801
50	0.205	0.206	0.781
60	0.184	0.195	0.735
70	0.143	0.168	0.63
80	0.077	0.111	0.397
90	0	0	0
hemispherical	0.192	0.196	0.74

4. Results

4.1. Heat Transfer

The output of (Eq. 16) does not distinguish whether the resulting rate of heat transfer over a given hour of NSRDB input corresponds to a heating or cooling load placed upon mechanical equipment. Since significant differences in efficiency commonly correspond to these space conditioning modes it is necessary to define criteria to allow the outputs to be categorized. For the sake of this study, heating loads are defined as those for which the exterior temperature is lower than the interior temperature and for which the rate of heat transfer attributed to the conductance of the wall exceeds solar gain. While this specification is well guided by intuition, changes in solar gain manifest by the application of coatings or replacement of uncoated glass with low-e will change the number of days that heating or cooling is applied since solar gain off-sets heat loss in the winter. This effect is exhibited in the data that will be discussed. It would be unforthcoming not to identify that ventilation, zone heating strategies, other loads and the thermal capacitance of a given building may also affect these balances. This is especially true in "Mediterranean" climates that invite nighttime ventilation or when internal loads are significant enough to diminish or exceed temperature-driven wintertime heat loss. In some

cases shading that is native to a given building due to its geographic location or position relative to other structures will greatly diminish solar loads. Thus, the outcomes of this study are applicable as guidelines which aid our intuition, but do not supersede highly detailed analysis that should be appropriately applied for a given building.

Table 3: Annual Rates of Heat Transfer for Each Orientation [Mbtu/yr-assembly]

Existing Façade Case

	North		East		South		West	
City	Heating	Cooling	Heating	Cooling	Heating	Cooling	Heating	Cooling
Minneapolis	8.15	3.35	8.01	7.49	7.58	12.12	7.85	8.61
Denver	6.28	4.43	6.12	12.15	6.01	15.91	6.12	12.15
New York	4.88	3.98	4.75	9.54	4.61	12.54	4.75	9.54
Seattle	5.84	2.73	5.77	6.78	5.70	9.67	5.80	6.95
Las Vegas	2.65	7.92	2.62	16.72	2.61	20.31	2.64	15.22
Miami	0.09	9.47	0.09	15.74	0.09	15.73	0.09	12.71

Renovated Façade Case

	North		East		South		West	
City	Heating	Cooling	Heating	Cooling	Heating	Cooling	Heating	Cooling
Minneapolis	9.25	1.07	8.84	2.14	8.40	2.70	9.05	2.01
Denver	7.17	1.70	6.77	3.39	6.46	4.11	6.77	3.39
New York	5.70	1.34	5.40	2.54	5.10	3.07	5.57	2.10
Seattle	6.88	0.53	6.65	1.39	6.44	1.96	6.76	1.54
Las Vegas	2.95	4.71	2.79	6.90	2.74	7.80	2.91	6.61
Miami	0.10	5.23	0.10	6.89	0.10	6.89	0.10	6.09

Retrofit Façade Case

	North		East		South		West	
City	Heating	Cooling	Heating	Cooling	Heating	Cooling	Heating	Cooling
Minneapolis	3.42	0.88	3.26	2.22	3.13	3.08	3.35	1.97
Denver	2.79	1.22	2.67	3.22	2.60	4.16	2.74	2.52
New York	2.24	1.07	2.15	2.51	2.06	3.24	2.19	1.94
Seattle	2.62	0.61	2.56	1.65	2.51	2.37	2.59	1.73
Las Vegas	1.16	2.61	1.13	4.94	1.12	5.86	1.15	4.57
Miami	0.04	3.03	0.04	4.70	0.04	4.68	0.04	3.90

(Table 3) indicates the annual rate of heat transfer calculated for each façade orientation based on NSRDB data for the city indicated for the year 2024. These values correspond to either a single façade unitized assembly in the case of “reclad” or an equivalent area for the other two cases in (Table 2). In general, cooling loads which are driven primarily by insolation, show the most variation with south facing orientations exhibiting the highest values. It is noteworthy that in Miami, the eastern and western exposures are also very high due to the high path of the sun during summer months near the equator which limits southern exposure more than in the other climates investigated. In many of the instances reported, east and west facing values exhibit some variation. This is the result of systematic weather patterns which vary in the manner that they affect sky clarity during different portions of the day. Heating loads exhibit less variation and are affected by heating demand that is offset by insolation. In fact, they would not exhibit any variation in absence of this effect since conductance and air infiltration do not observe building orientation as an Input.

(Figs. 4 and 5) are derived from the data of (Table 3) for the sake of simplifying a comparative assessment of the results. In these figures, the values for each cardinal orientation are averaged to provide a single value for each city and treatment. Loads that correspond to heating shown in (Fig. 4) are the highest for the case that the façade is renovated since improving the solar control of the system by application of an applied film diminishes the benefit of solar heating during wintertime months. This increase is grossly exceeded by the reduction in cooling demand during summertime months

which is apparent in (Fig. 5) for the same treatment. A large drop in heating demand is achieved by façade retrofit since wintertime heat loss is U-factor driven. Improvements in cooling loads are only modest if renovations to improve solar control have already been performed. In terms of gross magnitude cooling loads tend to be somewhat higher than heating loads, even in heating climates. While this is implicitly true in mild climates it is important to consider the fact that cooling systems exhibit efficiencies exceeding combustion heat sources and most buildings benefit from some form of shading whether it be a consequence of design or the result of surroundings. Subsequently the cooling energy indicated is a worst case scenario and may be less carbon-intensive to mitigate.

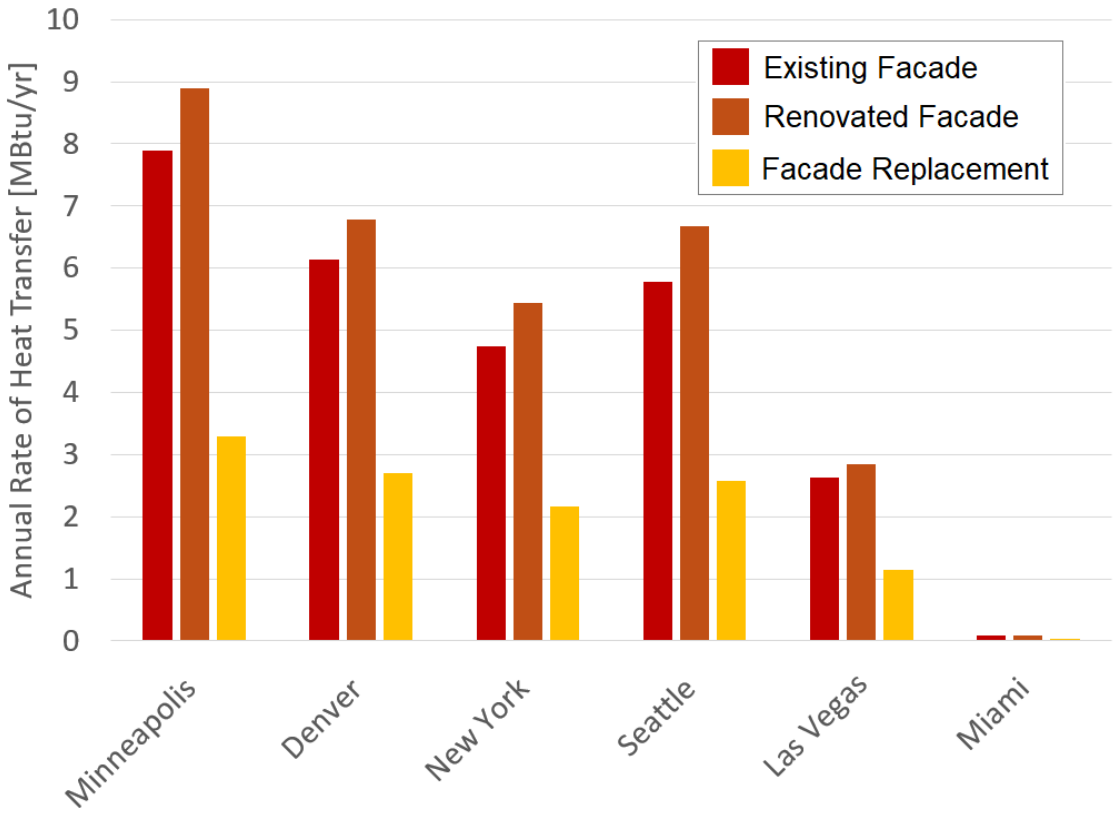

Fig. 4: (Heating Condition) Modeled Annual Temperature Driven Heat Transfer Not Offset by Insolation Averaged for North, East, West and South Façade Orientations for the 2024 Calendar Year.

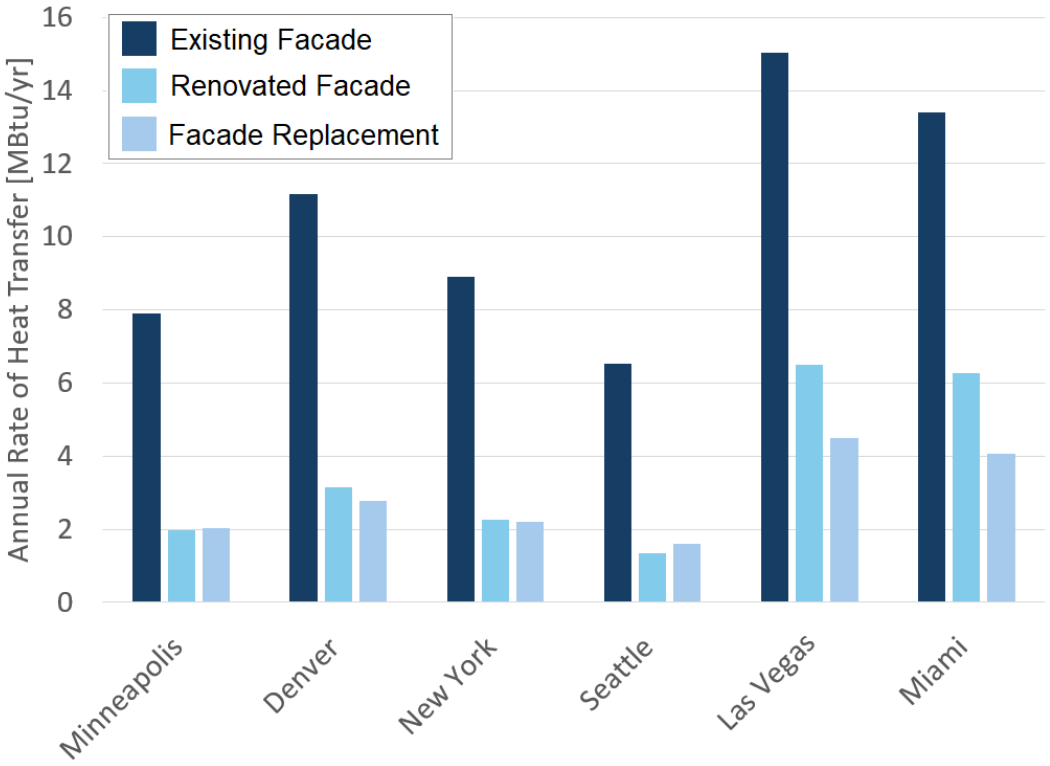

Fig. 5: (Cooling Condition) Modeled Annual Insolation Driven Heat Transfer Not Employed to Offset Heating Averaged for North, East, West and South Façade Orientations for the 2024 Calendar Year.

4.2. Operational vs. Embodied Carbon

As described in the preceding sections, the system chosen for analysis (ES-EPD1044) was selected since both its thermal properties and global warming potential have been established and are familiar to the author. Specifically, the GWP of a 5' x 15' assembly is approximately 1,600 $kgCO_{2,\,equiv}$ per curtain wall assembly. Other values of environmental interest are provided in (Fig. 6).

It is noteworthy that thermal properties of custom fabricated curtain wall systems are routinely determined for coordination with validation efforts for a given project, but are not always openly published since they are not intended for generic applications. This is not a barrier to conducting studies of the nature reported here since most manufacturers would provide this information for a given proposed project in accordance with bid solicitations. The best records that are publicly available to underpin further analysis correspond to standard, "off the shelf" products which are sometimes suitable for retrofit applications. Care should be exercised in ensuring that performance values observed match the intended installation which can be affected by transitions between wall systems, vision areas and opaque wall that are not always represented in product literature. In particular, the size of the assembly in width and height should match the intended application. Availability of EPD data to underpin embodied carbon is currently available for select wall systems and is not limited to the single case reported here; however, the availability of product data is currently somewhat sparse. This reality will likely change in the United States due to evolving code requirements and the desires of building owners. The system chosen for this study was selected for the convenience of the author; however, the results conveyed would likely be applicable to similar wall designs that are responsibly sourced.

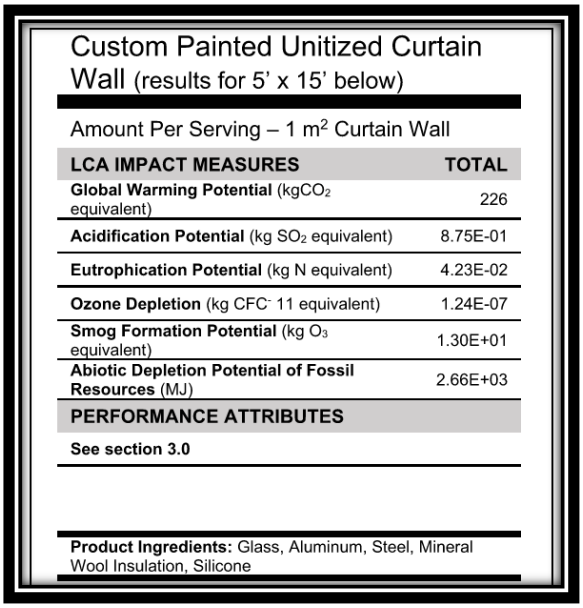

Custom Painted Unitized Curtain Wall (results for 5' x 15' below)

Amount Per Serving – 1 m^2 Curtain Wall

LCA IMPACT MEASURES	TOTAL
Global Warming Potential ($kgCO_2$ equivalent)	226
Acidification Potential (kg SO_2 equivalent)	8.75E-01
Eutrophication Potential (kg N equivalent)	4.23E-02
Ozone Depletion (kg CFC^- 11 equivalent)	1.24E-07
Smog Formation Potential (kg O_3 equivalent)	1.30E+01
Abiotic Depletion Potential of Fossil Resources (MJ)	2.66E+03
PERFORMANCE ATTRIBUTES	
See section 3.0	

Product Ingredients: Glass, Aluminum, Steel, Mineral Wool Insulation, Silicone

Fig. 6: Environmental Product Declaration Data for ES EPD1044.

In order to accomplish the aim of calculating a "carbon buy back period" that establishes how long it would take for operational carbon savings to equate to the quantity of carbon produced by conducting retrofit activities, carbon factors for utility energy must be established for the sake of correlating energy expenditures. It is also necessary to establish the efficiency of heating and cooling systems. It is noteworthy that cooling systems and heat pumps routinely exhibit electrical efficiencies in relation to the quantity of heat displaced that exceeds 100% because the energy required to move heat between thermal reservoirs is less than the quantity of heat transferred. This reality is reflected in the coefficient of performance COP which defines this ratio of cooling output to work input. To ease computations it is commonplace in the United States to express a similar relationship defined as an energy efficiency ratio (EER); whereby, the cooling capacity is expressed in [BTU/hr] and the energy input is defined in Watts as shown in (Eq. 17.)

Heating is a direct energy conversion process when fossil fuels are combusted to generate heat. These processes cannot exceed 100% conversion efficiency of the energy stored in the fuel source, although modern heating systems operate near this efficiency. Historically, the conversion efficiency of combustion-based heating systems has been much lower with values as low as 65% for aging boiler based systems typical of large buildings.

$$EER = \frac{Cooling\ Output\ [Btu/hr]}{Electric\ Power\ Consumption\ [Watts]} \qquad \text{Eq. 17}$$

Carbon coefficients for fuel sources vary geographically. Especially when considering sources of electric power which can vary significantly depending on the extent to which renewable energy sources are incorporated into a given distribution network. It is noteworthy that as an aggregate the carbon coefficient corresponding to electrical utility power in the United States is currently higher than certain fossil fuels, in particular natural gas. This is the case because electric power generation still relies upon coal for a significant portion of its capacity. According to data published in 2023 by the Environmental Information Administration (EIA) the value stood at 16% (EIA, 2026). Carbon coefficients for electric utilities observed in this study were obtained from the Environmental Protection Agency (EPA) in accordance with the eGrid designation for each city analyzed (EPA, 2026). These values vary from

0.274 to 0.511 [$kgCO_{2equiv}$/Kwh]. Carbon coefficients for combustible fuel sources employed in the study assumed a value of 5.3E-05[$kgCO_{2equiv}$/MBtu] for natural gas and 7.5E-05[$kgCO_{2equiv}$/MBtu] for fuel oil. These values reflect those published by the EIA and which are observed in LL97 (City of New York, 2019).

Table 4: Average Reduction in GWP Achieved by Façade Replacement Exceeding Façade Renovation Per Curtain Wall Assembly

	Heating					Cooling					Net	
City	Heating Efficiency	Fuel Source	Carbon Coeff. [$kgCO_{2eq}$ /MBtu]	Δ Annual Q [Mbtu /yr]	Δ Annual GWP [$kgCO_{2eq}$ /yr]	Cooling EER	Fuel Source	Carbon Coeff. [$kgCO_{2eq}$ /kWh]	Δ Annual P [kWh /yr]	Δ Annual GWP [$kgCO_{2eq}$ /yr]	Δ Net Reduction GWP [$kgCO_{2eq}$ /yr]	Carbon Payback t [yr]
Minneapolis	65	Natural Gas	5.3E-05	8,605,124.13	457.02	8	Electricity	0.426	-7.03	-3.00	454.02	3.5
Minneapolis	65	Fuel Oil	7.5E-05	8,605,124.13	645.38	8	Electricity	0.426	-7.03	-3.00	642.39	2.5
Minneapolis	95	Natural Gas	5.3E-05	5,887,716.51	312.70	15	Electricity	0.426	-3.75	-1.60	311.10	5.1
Minneapolis	95	Fuel Oil	7.5E-05	5,887,716.51	441.58	15	Electricity	0.426	-3.75	-1.60	439.98	3.6
Denver	65	Natural Gas	5.3E-05	6,290,908.67	334.11	8	Electricity	0.511	45.93	23.47	357.58	4.5
Denver	65	Fuel Oil	7.5E-05	6,290,908.67	471.82	8	Electricity	0.511	45.93	23.47	495.29	3.2
Denver	95	Natural Gas	5.3E-05	4,304,305.93	228.60	15	Electricity	0.511	24.49	12.52	241.12	6.6
Denver	95	Fuel Oil	7.5E-05	4,304,305.93	322.82	15	Electricity	0.511	24.49	12.52	335.34	4.8
New York	65	Natural Gas	5.3E-05	5,050,014.53	268.21	8	Electricity	0.402	9.05	3.64	271.84	5.9
New York	65	Fuel Oil	7.5E-05	5,050,014.53	378.75	8	Electricity	0.402	9.05	3.64	382.39	4.2
New York	95	Natural Gas	5.3E-05	3,455,273.10	183.51	15	Electricity	0.402	4.82	1.94	185.45	8.6
New York	95	Fuel Oil	7.5E-05	3,455,273.10	259.15	15	Electricity	0.402	4.82	1.94	261.08	6.1
Seattle	65	Natural Gas	5.3E-05	6,326,155.01	335.98	8	Electricity	0.274	-29.22	-8.00	327.98	4.88
Seattle	65	Fuel Oil	7.5E-05	6,326,155.01	474.46	8	Electricity	0.274	-29.22	-8.00	466.46	3.43
Seattle	95	Natural Gas	5.3E-05	4,328,421.85	229.88	15	Electricity	0.274	-15.58	-4.27	225.61	7.09
Seattle	95	Fuel Oil	7.5E-05	4,328,421.85	324.63	15	Electricity	0.274	-15.58	-4.27	320.36	4.99
Las Vegas	65	Natural Gas	5.3E-05	2,627,759.62	139.56	8	Electricity	0.353	251.08	88.63	228.19	7.01
Las Vegas	65	Fuel Oil	7.5E-05	2,627,759.62	197.08	8	Electricity	0.353	251.08	88.63	285.71	5.60
Las Vegas	95	Natural Gas	5.3E-05	1,797,940.79	95.49	15	Electricity	0.353	133.91	47.27	142.76	11.21
Las Vegas	95	Fuel Oil	7.5E-05	1,797,940.79	134.85	15	Electricity	0.353	133.91	47.27	182.11	8.79
Miami	65	Natural Gas	5.3E-05	92,338.11	4.90	8	Electricity	0.370	275.01	101.75	106.66	15.00
Miami	65	Fuel Oil	7.5E-05	92,338.11	6.93	8	Electricity	0.370	275.01	101.75	108.68	14.72
Miami	95	Natural Gas	5.3E-05	63,178.70	3.36	15	Electricity	0.370	146.67	54.27	57.62	27.77
Miami	95	Fuel Oil	7.5E-05	64,715.09	4.74	15	Electricity	0.370	146.67	54.27	59.01	27.12

(Tables 4 and 5) indicate annual improvements in operational GWP obtained through façade retrofit respectively for the case where renovations have already been employed and for which no renovations were performed as detailed in (Table 2). In each instance the efficiency of the heating system and its fuel type are varied to consider a low performing option and a mechanical system with modest efficiency improvements. In the former case the efficiency of combustion-based heating is 65% and the EER of electric utility based cooling is EER 8. The latter case assumes 95% combustion efficiency and an EER rating of 15. The combustion fuel sources considered are fuel oil and natural gas. The final column, the carbon payback period, in both tables indicates the period over which the embodied carbon associated with the façade unit is compensated by a reduction in operational carbon.

Table 5: Average Reduction in GWP Achieved by Façade Replacement Exceeding Existing Installation Per Curtain Wall Assembly

	Heating					Cooling					Net	
City	Heating Efficiency	Fuel Source	Carbon Coeff. [$kgCO_{2eq}$ /MBtu]	Δ Annual Q [Mbtu /yr]	Δ Annual GWP [$kgCO_{2eq}$ /yr]	Cooling EER	Fuel Source	Carbon Coeff. [$kgCO_{2eq}$ /kWh]	Δ Annual P [kWh /yr]	Δ Annual GWP [$kgCO_{2eq}$ /yr]	Δ Net Reduction GWP [$kgCO_{2eq}$ /yr]	Carbon Payback t [yr]
Minneapolis	65	Natural Gas	5.3E-05	7,087,348.64	376.41	8	Electricity	0.426	732.00	311.83	688.24	2.3
Minneapolis	65	Fuel Oil	7.5E-05	7,087,348.64	531.55	8	Electricity	0.426	732.00	311.83	843.38	1.9
Minneapolis	95	Natural Gas	5.3E-05	4,849,238.55	257.54	15	Electricity	0.426	390.40	166.31	423.85	3.8
Minneapolis	95	Fuel Oil	7.5E-05	4,849,238.55	363.69	15	Electricity	0.426	390.40	166.31	530.00	3.0
Denver	65	Natural Gas	5.3E-05	5,279,425.89	280.39	8	Electricity	0.511	1047.51	535.28	815.67	2.0
Denver	65	Fuel Oil	7.5E-05	5,279,425.89	395.96	8	Electricity	0.511	1047.51	535.28	931.24	1.7
Denver	95	Natural Gas	5.3E-05	3,612,238.77	191.85	15	Electricity	0.511	558.67	285.48	477.33	3.4
Denver	95	Fuel Oil	7.5E-05	3,612,238.77	270.92	15	Electricity	0.511	558.67	285.48	556.40	2.9
New York	65	Natural Gas	5.3E-05	3,981,813.18	211.47	8	Electricity	0.402	838.94	337.25	548.73	2.9
New York	65	Fuel Oil	7.5E-05	3,981,813.18	298.64	8	Electricity	0.402	838.94	337.25	635.89	2.5
New York	95	Natural Gas	5.3E-05	2,724,398.49	144.69	15	Electricity	0.402	447.43	179.87	324.56	4.9
New York	95	Fuel Oil	7.5E-05	2,724,398.49	204.33	15	Electricity	0.402	447.43	179.87	384.20	4.2
Seattle	65	Natural Gas	5.3E-05	4,930,119.00	261.84	8	Electricity	0.274	617.92	169.31	431.15	3.71
Seattle	65	Fuel Oil	7.5E-05	4,930,119.00	369.76	8	Electricity	0.274	617.92	169.31	539.07	2.97
Seattle	95	Natural Gas	5.3E-05	3,373,239.32	179.15	15	Electricity	0.274	329.55	90.30	269.45	5.94
Seattle	95	Fuel Oil	7.5E-05	3,373,239.32	252.99	15	Electricity	0.274	329.55	90.30	343.29	4.66
Las Vegas	65	Natural Gas	5.3E-05	2,295,284.59	121.90	8	Electricity	0.353	1318.29	465.36	587.26	2.72
Las Vegas	65	Fuel Oil	7.5E-05	2,295,284.59	172.15	8	Electricity	0.353	1318.29	465.36	637.50	2.51
Las Vegas	95	Natural Gas	5.3E-05	1,570,457.87	83.41	15	Electricity	0.353	703.09	248.19	331.60	4.83
Las Vegas	95	Fuel Oil	7.5E-05	1,570,457.87	117.78	15	Electricity	0.353	703.09	248.19	365.97	4.37
Miami	65	Natural Gas	5.3E-05	79,649.34	4.23	8	Electricity	0.370	1166.66	431.67	435.90	3.67
Miami	65	Fuel Oil	7.5E-05	79,649.34	5.97	8	Electricity	0.370	1166.66	431.67	437.64	3.66
Miami	95	Natural Gas	5.3E-05	54,496.92	2.89	15	Electricity	0.370	622.22	230.22	233.12	6.86
Miami	95	Fuel Oil	7.5E-05	64,715.09	4.09	15	Electricity	0.370	622.22	230.22	234.31	6.83

Reductions in carbon emissions correlate both with climatic factors, fuel sources and mechanical system efficiency. It is noteworthy that the improvements described in the case where only renovations are performed that the solar control properties of the system are improved; however, there is no significant improvement in the U-factor of the existing installation. It follows, as a general principle, that reducing solar loads is generally less costly and complicated than improving system U-factors which commonly requires more invasive work. Observing the GWP values for Miami in both (Table 4 and 5) illustrates this point. Complete façade replacement with poor performing mechanical systems would accomplish parity in as little as 4 years; however, the majority of this impact is owed to the fact that solar enhancements have been introduced. If improvements and solar control and system efficiency have already been implemented, the time required to achieve parity increases considerably. This is apparent in (Table 5) with values of approximately 14 years and more than 25 years when these improvements are considered in succession. Therefore, it can reasonably be concluded that façade retrofit is a less efficient carbon reduction strategy for buildings with energy demands that are driven by insolation alone. Alternatively, in heating climates the time required for the embodied carbon associated with retrofit are relatively short. In Minneapolis this value barely exceeds five years even when renovation has already been performed. In this scenario improvement of the system U-factor is the only viable way to substantially reduce heating loads. In fact, increased shading and solar control have a counterproductive affect during heating periods due to the fact that solar gain provides a benefit.

Variations in GWP associated with heating fuel sources and system efficiency vary in a predictable fashion. Since cooling system efficiencies vary more greatly than combustion-based sources the outcomes for heating climates are less sensitive to these parameters than they are for cooling climates. It is worth noting that certain values in table 4 report negative values in the cooling. This is a consequence of the criteria employed to define heating and cooling loads. Improving the U-factor of the system through retrofit reduces temperature driven heat transfer and subsequently there are more days in a given year that solar gain exceeds temperature driven heat loss. Thus, those days are

defined as satisfying the criteria for being accounted as a cooling condition. The reduction does not reflect the solar control properties of the system being diminished. This should be regarded as an artifact of the assumptions of the study.

4.3. Concluding Remarks

The study presented here employs finite element software programs that are conventionally used in the United States to determine the thermal properties of a modern unitized curtain wall system for which the product embodied GWP has been established by mean of a lifecycle assessment. The thermal performance data was used in conjunction with NSRDB weather data and a solar model to examine the net energy balance on the façade unit over the period of a year in different climates and orientations. Additionally two theoretical scenarios were proposed with thermal properties corresponding to an aging system with poor thermal performance and a system employing common façade renovations such as the application of solar control film and sealant work. The energy balances for these scenarios and the modern curtain wall system were compared to examine the impact of the improvements on façade heat transfer. Additionally, a sensitivity study was conducted to link the heat transfer values to GWP by mean of carbon coefficients and assumed mechanical system efficiencies. Mechanical systems employed combustion based fuel sources for heating and electric cooling. It was determined that in all cases improvements in operational carbon offset the GWP associated with the unitized curtain wall system within thirty years. The specific “carbon buy back period” defined in the context of these outcomes is provided for each case. In the vast majority of cases, the time required to achieve carbon parity was less than ten years. Of these cases, façade retrofit was found to be the most viable carbon reduction strategy in strong heating climates since the improvements in system U-factor are difficult to accomplish by other means. It was also found, that improvements to combustion based heating systems are less effective in these climates than improvements in cooling systems since cooling system efficiencies tend to achieve higher values. Façade retrofit was found to be less effective in cooling climates with mild winters since, solar control strategies are easier to apply as a renovation.

References

[1] Mark Lynas, et. al: Greater than 99% consensus on human caused climate change in peer-reviewed scientific literature : Environ. Res. Lett. 16, 7 pp (2021)

[2] H. Pörtner, et. al.: IPCC, 2022: Climate Change 2022: Impacts, Adaptation and Vulnerability: Contribution of Working Group II to the Sixth Assessment Report of the Intergovernmental Panel on Climate Change. Cambridge University Press, 3056 pp (2022)

[3] Local Law 97 of the City of New York: NYC Administrative Code § 28-320.1 et seq. https://www.nyc.gov/assets/buildings/local_laws/ll97of2019.pdf (2019)

[4] The Buy Clean California Act (BCCA): Public Contract Code §§ 3500-3505 https://www.dgs.ca.gov/pd/resources/page-content/procurement-division-resources-list-folder/buy-clean-california-act (2022)

[5] Thanyalak Srisamranrungruang and Kyosuke Hiyama: Life carbon assessment of embodied and operational carbon with view assessment across facade systems in Japanese climate zones: Rineng v. 29 (2026)

[6] Méndez Echenagucia, et. al. On the Tradeoffs between Embodied and Operational Carbon in Building Envelope Design: The Impact of Local Climates and Energy Grids: Energy Build. v. 278 (2023)

[7] Rosanna O’Neill, et. al. Integrated operational and life-cycle modelling of energy, carbon and cost for building façades: J. Clean. Prod v. 286 (2021)

[8] Roberto Giordano, et. al. Embodied energy and operational energy evaluation in tall buildings according to different typologies of façade: Energy Procedia v. 134 (2017)

[9] 90.1-2022—Energy Standard for Sites and Buildings Except Low-Rise Residential Buildings: ASHRAE (2022)

[10] ASTM C1199-22 - Standard Test Method for Measuring the Steady-State Thermal Transmittance of Fenestration Systems Using Hot Box Methods: ASTM (2022)

[11] NFRC/ANSI 100-2023 - Procedure for Determining Fenestration Product U-factors: NFRC, ANSI (2023)

[12] ISO15099:2023 - Thermal performance of windows, doors and shading devices — Detailed calculations: ISO (2022)

[13] Software Tools Webpage: https://windows.lbl.gov/software-tools: Lawrence Berkeley National Laboratory - Windows and Daylighting Group (2026)

[14] NFRC/ANSI 300-2023 - Test Method for Determining the Solar Optical Properties of Glazing Materials and Systems: NFRC, ANSI (2023)

[15] ISO9845:2022 - Solar energy — Reference solar spectral irradiance at the ground at different receiving conditions: ISO (2022)

[16] J. E. Hay and J. A. Davies. Calculation of the Solar Radiation Incident on an Inclined Surface: Proceedings of First Canadian Solar Radiation Data Workshop: Toronto: (1980)

[17] National Solar Radiation Database Webpage: https://nsrdb.nrel.gov/: National Renewable Energy Laboratory, United States Department of Energy (2026)

[18] ASTM E779-19 - Standard Test Method for Determining Air Leakage Rate by Fan Pressurization: ASTM (2019)

[19] ES EPD1044 – Custom Painted Aluminum Curtain Wall: ICC Evaluation Service (2021)

[20] Frequently Asked Questions - What is U.S. electricity generation by energy source?: https://www.eia.gov/tools/faqs/faq.php?id=427&t=3: United States Energy Information Administration (2026)

[21] Greenhouse Gas Equivalencies Calculator - Calculations and References: https://www.epa.gov/energy/greenhouse-gas-equivalencies-calculator-calculations-and-references: United States Environmental Protection Agency (2026)

Challenging Glass Conference Proceedings – Volume 10 – June 2026 – Louter, Bos & Belis (Eds.)
International Conference on the Architectural and Structural Application of Glass
Challenging Glass Conference 10 – 15-17 June 2026 – TU Delft – The Netherlands

Platinum Sponsor

SAINT-GOBAIN

Gold Sponsors

EASTMAN

kuraray

NorthGlass®

sedak

seele

Silver Sponsors

DOW®

octatube

PERMASTEELISA GROUP

SEEN

Organisation

TU Delft

Technische Universität München

GHENT UNIVERSITY